

Modification of Drag-reduced Flow by dosing water from the wall - Investigation of Turbulent Structure by PIV-

Yuichiro IWAKI, Masaaki MOTOZAWA, Takahiro TSUKAHARA and Yasuo KAWAGUCHI

Department of Mechanical Engineering
Tokyo University of Science
2641 Yamazaki, Noda-shi, Chiba-ken, Japan
yasuo@rs.noda.tus.ac.jp

ABSTRACT

Experimental investigation of modified drag-reduced channel flow by covering the near-wall region with pure water was carried out. To modify the near-wall turbulent structure of drag-reduced channel flow of surfactant solution, the wall-dosing apparatus, in which pure water is supplied from the porous surface of the channel wall into the viscoelastic bulk flow, was used. By covering the near-wall region with water, drag reduction rate is slightly enhanced, compared with the viscoelastic channel flow without water dosing. We examined the mechanism of this enhancement of drag reduction and the change of the turbulent structure by water dosing from instantaneous velocity fields captured by PIV. The decomposition of C_f shows that viscoelastic stress decreases largely while Reynolds shear stress increases, which causes drag reduction to be enhanced. Moreover, characteristic turbulent structures were observed in the instantaneous velocity fields. In the near-wall region of this flow, the feature as usually reported in Newtonian fluid wall turbulence was observed and dosed water acts as a promoter of turbulence, which destabilize the flow of the viscoelastic fluid. On the other hand, away from the wall the feature is the one usually observed in drag-reduced flow and dosed water acts as a passive scalar because the mean concentration of dosed water is too small to destabilize the viscoelastic flow.

INTRODUCTION

The addition of certain kinds of surfactant additives to turbulent flow can obviously reduce the skin frictional drag. If this drag-reducing effect can be applied to some industrial situations, it has great potential to lead to energy saving. Therefore, a lot of studies to clarify the mechanism of this drag-reducing effect have been conducted and found that turbulent structures in the near-wall region have a great influence on the drag reduction (Iwamoto et al., 2005). However, despite a lot of studies, it still remains unclear how coherent structures in the near-wall region affect the drag-reducing effect. In our previous study (Motozawa et al., 2012) we experimentally investigated water channel flow covered the near-wall region with polymer solution by wall-dosing method, and revealed that Reynolds shear stress decreases and large drag reduction rate appears.

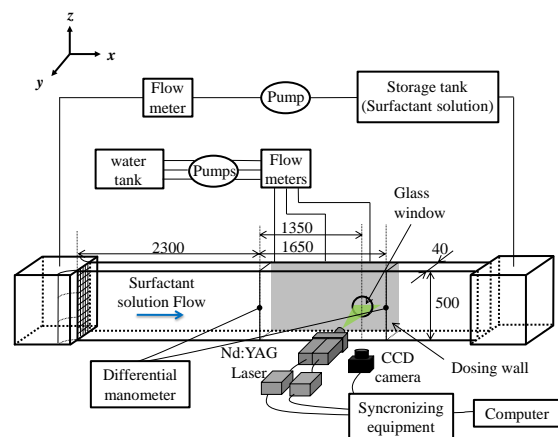


Fig. 1 Experimental apparatus.

To investigate the role for the near-wall turbulent structure in drag reduction in more detail, we investigated the near-wall coherent structure of modified viscoelastic channel flow by covering only the near-wall region with water (Newtonian fluid) in this study. This flow situation is the opposite to reducing drag by covering the near-wall region with polymer solution in our previous study. For investigation of the turbulent structure, PIV measurement was employed to measure the velocity field of this modified drag-reduced flow. On the basis of the results of PIV measurement, the affection of covering the near-wall region with water in a drag-reduced flow to turbulent structure was discussed.

EXPERIMENT APPARATUS

Figure 1 shows the experimental apparatus. The experiment was performed in a closed-circuit water loop with a 2D channel with a length of 6000 mm, width of 500 mm and height of 40 mm. The stainless mesh wall for dosing water into the channel flow, which was 1650 mm × 500 mm in size, was attached to one side of the channel in the x - z plane. Two pressure taps were installed on the opposite side wall of the dosing wall at distances 2300 and 3950 mm downstream from the channel entrance. Thus, Drag reduction rate (DR%) and frictional velocity u_τ could be calculated from the pressure drop.

40 ppm of CTAC (Cetyltrimethyl ammonium chloride) water solution was used as the drag-reducing

fluid, and water was dosed into this drag-reduced flow from the whole surface of the dosing wall at three patterns of dosing rate $Q_d=3, 6, 9$ L/min. In these conditions, the dosing velocities normal to the dosing wall V_w were 8.9×10^{-5} m/s, 1.8×10^{-4} m/s and 2.7×10^{-4} m/s, respectively. The temperature of the CTAC water solution and dosed water were stabilized at 25 ± 0.1 °C. The Reynolds number is defined with the channel height H and bulk mean velocity U_b and set at 17800 for the water channel flow and 18400 for the viscoelastic channel flow.

PIV measurement was carried out in the x - y plane 3650 mm downstream from the channel entrance. For PIV measurement, flow was seeded using Polyethylene powder as tracer particles. These particles were $20 \mu\text{m}$ in nominal mean diameter and had a specific gravity to water of 0.92. The PIV images were analyzed using the cross-correlation technique. Turbulence statistics were calculated from 500 frames, in which there were 49000 vectors (98 vectors at each y -position in one frame \times 500 frames) at each y -position.

RESULTS AND DISCUSSION

Drag Reduction Rate

DR% was defined by the following equation;

$$DR(\%) = \frac{\tau_n - (\tau_w - \tau_d)}{\tau_n} \times 100 \quad (1)$$

where, τ_n and τ_w are the wall shear stress of the drag-reduced channel flow of viscoelastic fluid without water dosing ($Q_d=0$ L/min) and with water dosing, respectively. τ_d is the wall shear stress of the water channel flow with dosing water. The relationship between DR% and Q_d is shown in Fig. 2. Regarding DR% measurements, we made experiments at $Re_b = 30000$ and 41000 in addition to $Re_b = 18400$. This result shows that DR% increases as Q_d increases, and eventually becomes saturated. A detailed discussion about this increment of DR% by water dosing will be made in later sections.

Streamwise velocity profile

The streamwise velocity profiles is shown in Fig. 3. U^+ is defined as mean velocity U normalized by frictional velocity u_τ and y^+ is defined as the position y normalized by u_τ/ν . In the case of viscoelastic channel flow without water dosing ($Q_d=0$ L/min), the mean velocity profiles are up-shifted in the log-law layer and have comparable high slope as with Virk's Asymptote (Virk et al., 1970). The velocity in the near-wall region is lower than that of water flow because of its high viscosity. In addition the slope of the velocity profiles decreases with increasing Q_d (i.e. increasing DR%). Generally, the velocity profile of the drag-reduced channel flow of homogeneous viscoelastic fluid is up-shifted and the slope increases with increasing DR%, which is the opposite tendency from the present study. The reason for this opposite tendency will be discussed in a later section.

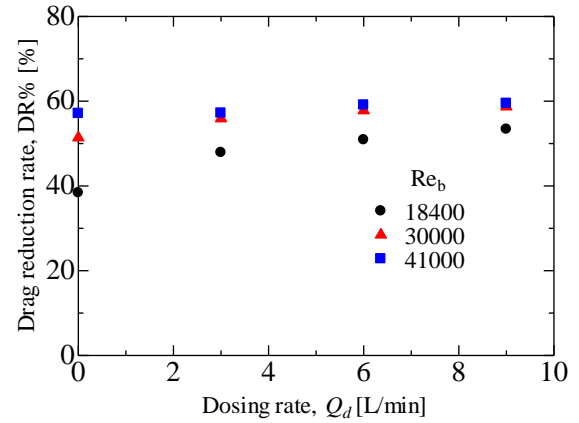


Fig. 2 Drag reduction rate DR% vs. Dosing rate Q_d .

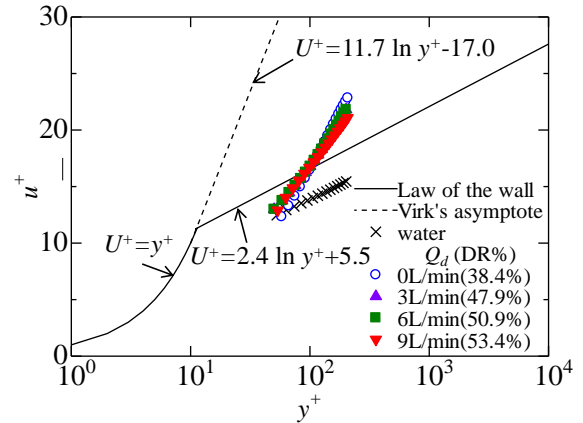


Fig. 3 Distribution of streamwise velocity.

Fractional contribution to C_f

We discuss the reason why drag reduction is enhanced by water dosing in this section. First, the total shear τ stress can be decomposed into the following three terms,

$$\tau = -\rho \overline{(-u'v')} + \tau_{VE} + \mu \frac{du}{dy} = \tau_T + \tau_{VE} + \tau_V \quad (2)$$

With supposing this flow should be developed, we normalize these three terms by τ_w and obtain with superscript⁺

$$\tau^+ = \tau_T^+ + \tau_{VE}^+ + \tau_V^+ = 1 - y^* \quad (3)$$

Fig. 3 shows the distributions of Reynolds shear stress, viscous stress and viscoelastic stress normalized by τ_w . Here, viscoelastic term can be calculated by subtracting the turbulent and the viscous stress from $1-y^*$. This figure shows that Reynolds shear stress increases in the near-wall region with increasing Q_d . In addition, this figure indicates that the viscoelastic stress is suppressed only in the near-wall region with increasing Q_d . FIK identity is proposed by Fukagata et al. (2002) as the following equation;

$$C_f = \frac{12}{Re_b} + 24 \int_0^1 (1-y^*) (-u'v') dy^* + 24 \int_0^1 (1-y^*) \tau^p dy^* \quad (4)$$

where, on the right side the first, the second and the third term are the viscous contribution, the turbulence contribution and the viscoelastic contribution, respectively. Therefore, the total contribution of Reynolds shear stress

and viscous stress to the frictional factor C_f can be calculated from the integral of each stress over y^* from 0 to 1. The calculation procedure of the viscoelastic contribution is as follows; C_f was calculated from the pressure drop, and both the turbulence contribution and viscous contribution were calculated from the PIV results. Therefore, the viscoelastic term can be calculated by subtracting the turbulence and the viscous contribution from C_f . Figure 4 shows the decomposition C_f into the turbulence contribution, the viscous contribution and the viscoelastic contribution for each flow condition.

The viscoelasticity of CTAC solution has both a positive role and a negative role in drag reduction phenomena. The positive role is the function of decreasing of skin frictional drag by decreasing Reynolds shear stress, while the negative one is the function of increasing skin frictional drag by appearing of viscoelastic stress. Generally, in viscoelastic turbulent flows a large drag reduction phenomena occurs because the decrement of the turbulence contribution is much larger than the increment of the viscoelastic contribution (Yu et al., 2004). However, in the present study, Fig. 4 clearly indicates that the decreasing level of viscoelastic contribution by covering the near-wall region with dosed water is larger than the increasing level of turbulence contribution. Therefore, DR% increases by water dosing, even though Reynolds shear stress increases.

Yu et al. performed a DNS study on the drag-reduced channel flow covered with water in the near-wall region, similar to the present study (Yu et al., 2005). The result showed that the Reynolds shear stress increased and DR% decreased. Therefore, their study is consistent with the present study in the point of the increment of Reynolds shear stress, however, it is different from the present study in regard to DR%. The reason for this difference seems to be the different in the thickness of near-wall water layer. In the case of their study, the water layer (i.e the Newtonian layer) was about ten times thicker than that in the present study. This thick water layer caused the turbulence contribution to C_f to be much larger than in the present study. Thus, because the increment of the turbulence contribution to C_f was larger than the decrement of the viscoelastic contribution to C_f , DR% decreased in their study.

Instantaneous velocity field

To discuss the behavior of the water channel flow, the viscoelastic channel flow without water dosing ($Q_d=0\text{L/min}$), and the viscoelastic channel flow with dosing ($Q_d=9\text{L/min}$), the instantaneous velocity field measured by PIV is examined in this chapter. Figures 5, 6, 7 and 8 correspond to the spatial distributions of streamwise velocity u^* , Reynolds shear stress $-u^*v^*/u_\tau^2$, swirling strength λci , and velocity gradient du^*/dy^* , respectively. In each figure, the case of the water channel flow, the viscoelastic channel flow without water dosing ($Q_d=0\text{L/min}$), and the viscoelastic channel flow water with dosing ($Q_d=9\text{L/min}$) are shown.

Spatial distribution of streamwise velocity. We discuss the behavior of each flow by comparing the spatial distributions of streamwise velocity in Figs 5.

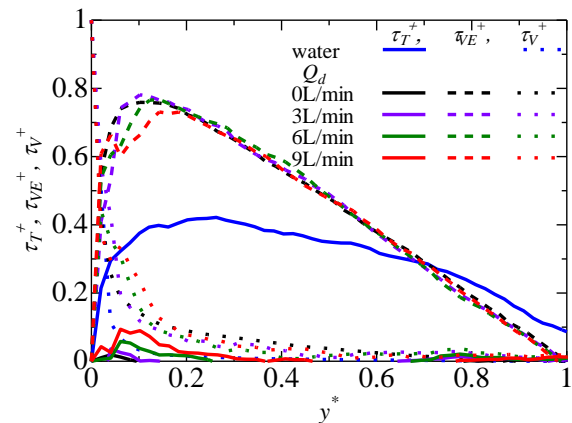


Fig. 3 Distribution of the shear stress balance.

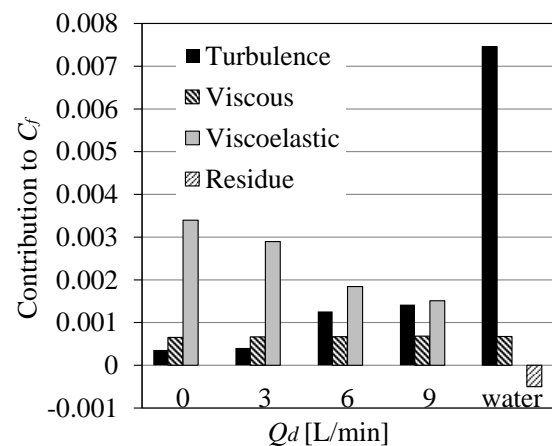


Fig. 4 Fractional contribution to C_f .

In the case of water channel flow shown in Fig. 5(a), larger velocity fluctuation in space than the others shown in Fig. 5(b) and Fig. 5(c) occurs at the same y position, by which contour lines drawn as a reference are curved irregularly. This feature indicates large-scale mixing of low speed and high speed fluid by coherent structures in the near-wall region as reported in usual wall turbulence.

In the case of a viscoelastic channel flow without water dosing ($Q_d=0\text{L/min}$) shown in Fig. 5(b), velocity fluctuation is not larger than that in the case of water at the same y position and the contour lines are almost parallel to the x axis. This indicates that coherent structures are suppressed and the mixing action of low and high speed fluids is inhibited by viscoelastic effect of the fluid, which matches the results in the past study (Li et al., 2008).

In the case of a viscoelastic channel flow with water dosing ($Q_d=9\text{L/min}$) shown in Fig. 5(c), the flow has quite different features between the near-wall region ($y^*<0.1$) and the region away from the wall ($y^*=0.4$). Although the contour lines are almost flat away from the wall, the contour lines are strongly curved in the near-wall region like the region marked by A. This feature indicates that low speed fluid in the near-wall region is destabilized by the dosed water and moved away from the wall, which causes large streamwise turbulent intensity to be produced in the near-wall region, the velocity profile to be down-shifted from viscoelastic channel flow without water

dosing ($Q_d=0\text{L/min}$) and the slope of the velocity profile to be lower in Fig. 3. Moreover, the streamwise scale of low speed fluid in $y^*<0.1$ is almost as large as the one in $y^*<0.1$ of water channel flow.

We also did a PLIF experiment to observe the diffusion of dosed water in the viscoelastic channel flow. The dosed water was dyed uniformly with Rhodamine-WT (6 ppm), and the dyed water was dosed into the drag-reduced channel flow with $Q_d=9\text{L/min}$. Figures 9 shows instantaneous PLIF images of the drag-reduced channel flow with dosing of dyed water at $Q_d = 9\text{ L/min}$. Both pictures (a) and (b) were measured in the same dosing condition after enough time for becoming steady flow had elapsed from the start of water dosing. These figures show that water and viscoelastic fluid are mixing in the region $0.1<y^*<0.4$. In the region $0.1<y^*<0.3$ of Figs. 9, curved structures such as velocity contour lines in the near-wall region in fig. 5(c) can be observed, and the velocity and concentration scales of these structures are similar. Therefore, the correspondence relationship between these structures of concentration and velocity is of interest.

Figure 10 shows a conceptual model of mixing dosed-dyed water into a viscoelastic flow. Dosed water in the instability region is lifted into the stability region by the ejection motions ($u'<0, v'>0$) caused by the instability, and irrupts into the higher speed region in which viscoelastic fluid is dominant ($0.1<y^*<0.3$). This irruption causes the high concentration region in Figs. 9, the curved velocity contour line and the low speed flow below the contour line in Fig. 5(c). The velocity fluctuation caused in this way is remarkable, especially in $y^*<0.1$. Dosed water further irrupts into the stability region in which viscoelastic fluid is dominant, and is stretched by the shear, and the filament structure in Figs. 9 is formed.

The above observations can be summarized as below. Dosed water in the viscoelastic channel flow has the feature of an active scalar, which changes the flow when it intrudes into the stable flow. In the region in which dosed water is dominant, the flow is destabilized and shows features which usually can be observed in Newtonian fluid turbulence. On the other hand, away from the wall, the mean concentration of dosed water (the concentration of dispersed water in the viscoelastic channel flow) is too small to destabilize the flow and dosed water behaves as a passive scalar. Therefore, velocity contour lines are flat and the pattern of dyed water is a regular filament shape stretched by the shear average flow. This transition region exists in $0.1<y^*<0.4$ in the present study.

Spatial distribution of instantaneous Reynolds shear stress. Spatial distributions of instantaneous Reynolds shear stress are shown in Figs. 6. In the case of water channel flow shown in Fig. 6(a) the irregular-shaped positive Reynolds shear stress region (marked by B) can be observed, which corresponds to ejection and sweep motions ($u'>0, v'<0$).

In the case of viscoelastic channel flow without water dosing ($Q_d=0\text{L/min}$) shown in Fig. 6(b) such a wide region where Reynolds shear stress has a high positive value cannot be observed, and negative and positive Reynolds shear stress with relatively weak strength occurs equally, which indicates that interaction motions ($u'<0,$

$v'<0$ or $u'>0, v'>0$) are as strong weight as ejection and sweep motions, and time-averaged Reynolds shear stress becomes almost zero. This large decrement in Reynolds shear stress is the reason of drag reduction.

In the case of a viscoelastic channel flow with water dosing ($Q_d=9\text{L/min}$) shown in Fig. 6(c), the region of strong positive Reynolds shear stress is observed in $y^*<0.1$, which induced by the destabilization, as mentioned in the previous section. In this region ($y^*<0.1$), the flow having a strong turbulent diffusion like that in a water channel flow is formed. In $0.1<y^*<0.3$, a larger area of positive Reynolds shear stress can be observed than that in the case without water dosing ($Q_d=0\text{L/min}$) in Fig. 6(b). This indicates this region ($0.1<y^*<0.3$) is the transitional region, in which the further away from the wall, the weaker influence as an active scalar the dosed water has. Even further away from the wall ($y^*>0.3$), Reynolds shear stress is quite small and its distribution is similar to that in Fig. 6(b).

Spatial distribution of swirling strength.

Swirling strength λci is proposed by Zhou et al. (1999) to visualize the vortex core. Vorticity can also be considered to determine whether a vortex exists; however, it is unsuitable for extracting only vortex cores because a position of high vorticity includes shear vortex, which is generated in the simple shear layer. On this point, swirling strength has the advantage of visualizing vortex because it extracts only vortex cores.

Spatial distributions of swirling strength are shown in Figs. 7. In the case of the water channel flow shown in Fig. 7(a), clockwise vortex cores (marked by C) correspond to the interface (marked by the dotted line) between the regions having large positive Reynolds shear stress (represented with red contour in Fig. 6(a)) and having negative one (represented with blue contour in Fig. 6(a)).

In the case of the viscoelastic channel flow without water dosing ($Q_d=0\text{L/min}$) shown in Fig. 7(b) concentrated vortex cores cannot be observed, and the positive (represented with red contour) and negative (represented with blue contour) swirling strength disperse evenly.

In the case of the viscoelastic channel flow with water dosing ($Q_d=9\text{L/min}$) shown in Fig. 7(c), strong clockwise vortex cores can be observed in $y^*<0.1$. These are induced by the destabilization of the water dosing.

Spatial distribution of instantaneous velocity gradient.

Spatial distributions of the instantaneous velocity gradient are shown in Figs. 8. In the case of the water channel flow shown in Fig. 8(a), the strong velocity gradient is concentrated only the near-wall region due to the typical turbulent velocity profile. In addition to this, the region with the high velocity gradient in the near-wall region of Fig. 8(a) exactly corresponds to the low speed region (represented with the blue contour) in Fig. 5(a) caused by organized structures in the near-wall region.

On the other hand, in the case of the viscoelastic channel flow without water dosing ($Q_d=0\text{L/min}$) shown in Fig. 8(b), the region with the strong velocity gradient is spread compared to that of Fig. 8(a). It is induced by the mean velocity characteristic of viscoelastic flow, which is shifted to the laminar-like profile because the viscoelastic fluids suppress the organized structure in the near-wall region.

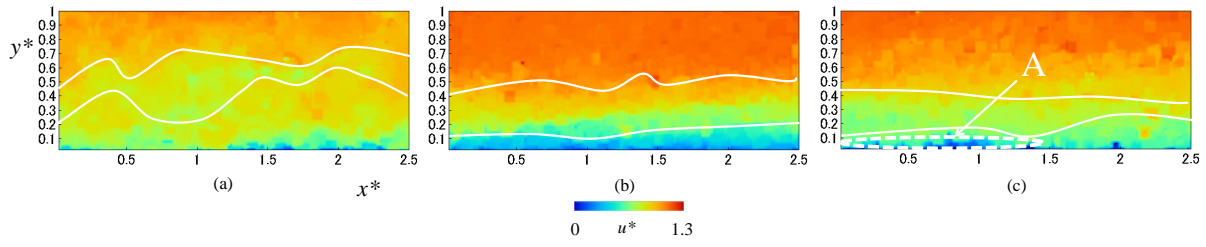


Fig. 5 Instantaneous distribution of streamwise velocity., (a) water channel flow, (b) viscoelastic channel flow without water dosing ($Q_d=0L/min$), and (c) viscoelastic channel flow with dosing ($Q_d=9L/min$)

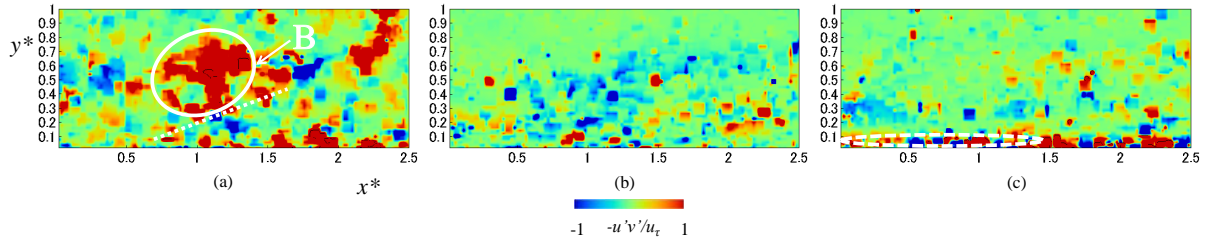


Fig. 6 Same as Fig. 5 but Instantaneous distribution of Reynolds shear stress.

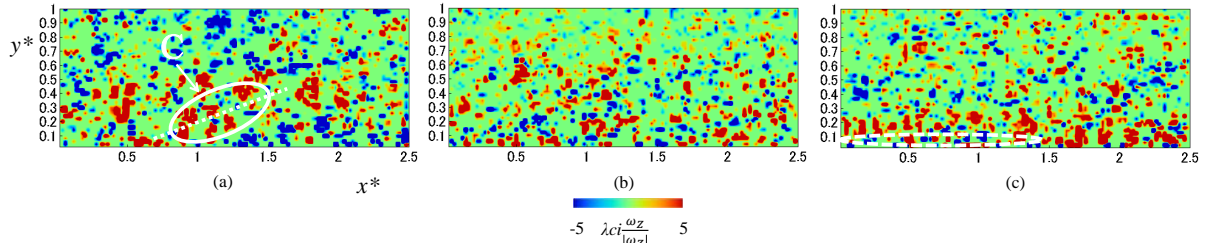


Fig. 7 Same as Fig. 5 but Instantaneous distribution of Swirling strength.

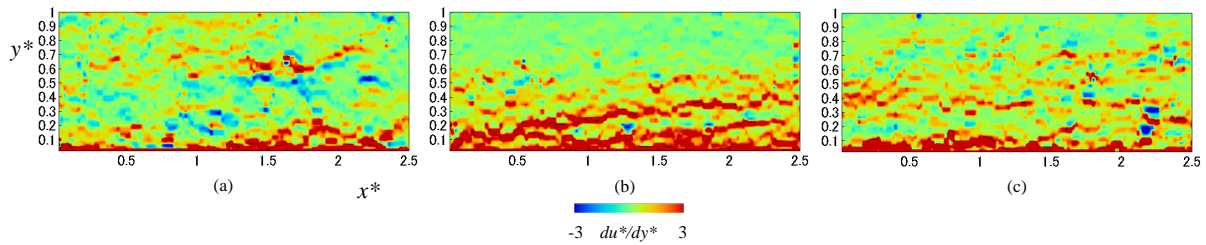


Fig. 8 Same as Fig. 5 but Instantaneous distribution of velocity gradient.



Fig. 9 PLIF images of dosing water to drag-reduced flow.

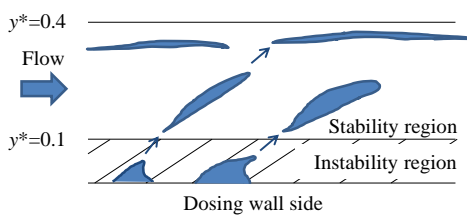


Fig. 10 Conceptual model of the generation of the filament structure in PLIF.

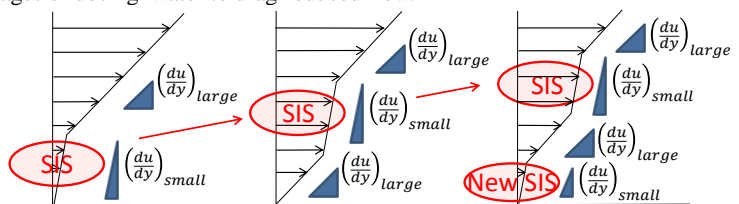


Fig. 11 Conceptual model of the streaky structure in velocity gradient.

In addition to that, it is of interest that the region represented by the red contour has a streaky pattern. Further discussion will follow in the next section.

In the case of the viscoelastic channel flow with water dosing ($Q_d=9\text{L/min}$) shown in Fig. 8(c), the strong velocity gradient in the near-wall region is observed. This high shear stress region is also observed in Fig. 8(a); however, away from the wall the streaky structure of the velocity gradient characterizing the viscoelastic fluid flow is similar to that in Fig. 8(b).

Based on the discussion above, it is concluded that the viscoelastic flow with water dosing has the features of Newtonian turbulence in the near-wall region while it has the feature of a drag-reduced flow away from the wall.

Spatial distribution of instantaneous velocity gradient and viscoelastic stress. In the viscoelastic channel flow without water dosing ($Q_d=0\text{L/min}$) shown in Fig. 8(b), it is of interest that the strong velocity gradient represented by the red contour has a streaky pattern with an inclination from the bottom left to the top right. Also, it can be observed that the distance between the streaks is small in the near-wall region; however, the further away from the wall, the larger the distance becomes. The mechanism for appearing of this streak is shown in Fig. 11.

It is reported that complex fluids like surfactant micellar solution, by which drag reduction occurs, show a physical property change caused by local shear deformation, which is called "Shear Induced State (SIS)", the fluid in SIS has higher viscoelasticity and higher viscosity than that in non-SIS. Therefore, when SIS occurs in a uniform stress field, a smaller velocity gradient is formed due to the high viscosity.

In a channel flow like that in the present study, the time-averaged velocity gradient is strong in the near-wall region and SIS can occur in the near-wall region first. Then the fluid lump in SIS shifts up from the wall. When the fluids reach the region with a low velocity gradient in the center of the channel, the fluids in SIS changes those in non-SIS by molecular motion. In this small velocity gradient region located between the streaks of strong velocity gradient, a zone of fluids in SIS exists and moves in the wall normal direction as mentioned above. Viscoelastic stress contributes to the shear stress in the similar way with Reynolds shear stress by this momentum transportation mechanism caused by the change in the material property of viscoelastic fluid /the velocity fluctuation correlation term. This viscoelastic contribution may explain why viscoelastic flow has more wall friction than laminar flow and turbulence is produced even if Reynolds shear stress drops to zero in a drag-reduced flow.

CONCLUSION

In this work, we discussed the turbulent structure in the viscoelastic flow modified in the near-wall region with by water dosing. In this modified flow, drag reduction rate is enhanced compared to the flow without water dosing despite Reynolds shear stress increases. Based on the decomposition of C_f with FIK identity, it is found that this contradictory feature is attributed to the large decrease of viscoelastic stress by water dosing.

The characteristic structures are shown in the spatial distributions of streamwise velocity, Reynolds shear stress and swirling strength. In the near-wall region of this

modified flow, the feature as usually observed in Newtonian fluid turbulence can be observed and dosed water acts as an active scalar, which changes the flow when it intrude into the stable flow. On the other hand, away from the wall, the feature as usually observed in drag-reduced flow can be observed and dosed water acts as a passive scalar because the mean concentration of dosed water is too small to destabilize viscoelastic flow.

In addition, it is of great interest that the viscoelastic channel flow without water dosing ($Q_d=0\text{L/min}$) has streaky patterns in the instantaneous distribution of velocity gradient. Those streaky patterns are induced by SIS (Shear Induced State), which is physical property change induced by local shear deformation and causes higher viscosity and viscoelasticity. When SIS occurs in a uniform stress field, a smaller velocity gradient is formed due to the high viscosity. And that is, those streaky structure (i.e. the smaller velocity gradient) indicates the appearing of fluids in SIS, which cause viscoelastic stress. In addition, the viscoelastic channel flow with water dosing ($Q_d=9\text{L/min}$) does not have those streaky patterns, which matches the decrease of viscoelastic stress on the decomposition of C_f .

REFERENCES

- Fukagata, K., Iwamoto, K. and Kasagi, N., 2002, "Contribution of Reynolds stress distribution to the skin friction in wall-bounded flows", *Physics of Fluids.*, vol. 14, pp. 73-76.
- Iwamoto, K., Fukagata, K., Kasagi, N. And Suzuki, Y., 2005, "Friction drag reduction achievable by near-wall turbulence manipulation at high Reynolds numbers", *Physics of Fluids.*, vol. 14, pp. 73-76.
- Li, F.-Ch., Kawaguchi, Y., Yu, B., Wei, J.-J. and Hishida, K., 2008, "Experimental study of drag-reduction mechanism for a dilute surfactant solution flow", *International Journal of Heat and Mass Transfer.*, vol. 51, pp. 835-843.
- Motozawa, M., Ishitsuka, S., Iwamoto, K., Ando, H., Senda, T. and Kawaguchi, Y., 2012, "Experimental Investigation on Turbulent Structure of Drag Reducing Channel Flow by Blowing Polymer Solution from the wall", *Flow, Turbulence and Combustion.*, vol. 88, pp. 121-141.
- Virk, P. S., Mickley, H. S. and Smith, K. A., 1970, "The Ultimate Asymptote and Mean Flow Structure in Toms' Phenomenon", *Journal of Applied Mechanics.*, vol. 37, pp. 480-493.
- Yu, B., Li, F.-Ch. and Kawaguchi, Y., 2005, "DNS of Drag-reducing Turbulent Channel Flow with Coexisting Newtonian and Non-Newtonian Fluid", *Journal of Fluids Engineering.*, vol. 127, pp. 929-935.
- Yu, B., Li, F.-Ch. and Kawaguchi, Y., 2004, "Numerical and experimental investigation of turbulent characteristics in a drag-reducing flow with surfactant additives", *International Journal of Heat and Fluid Flow.*, vol. 25, pp. 961-974.
- Zhou, J., Adrian, R. J., Balachandar, S. and Kendall, T. M., 1999, "Mechanisms for generating Coherent Packets of Hairpin Vortices in the Near-wall Turbulence", *Journal of Fluid Mechanics.*, vol. 387, pp. 353-396.